Berkeley 51, a young open cluster with four yellow supergiants

I. Negueruela,[1]⋆ M. Monguió,[1,2] A. Marco,[1] H. M. Tabernero,[1]
C. González-Fernández[3] and R. Dorda[1]

[1]*Departamento de Física, Ingeniería de Sistemas y Teoría de la Señal, Universidad de Alicante, Carretera San Vicente del Raspeig s/n, E-03690 San Vicente del Raspeig, Spain*
[2]*School of Physics, Astronomy and Mathematics, University of Hertfordshire, College Lane, Hatfield, Hertfordshire AL10 9AB, UK*
[3]*Institute of Astronomy, University of Cambridge, Madingley Road, Cambridge CB3 0HA, UK*

ABSTRACT

The heavily obscured open cluster Berkeley 51 shows characteristics typical of young massive clusters, even though the few previous studies have suggested older ages. We combine optical (*UBV*) and 2MASS photometry of the cluster field with multi-object and long-slit optical spectroscopy for a large sample of stars. We apply classical photometric analysis techniques to determine the reddening to the cluster, and then derive cluster parameters via isochrone fitting. We find a large population of B-type stars, with a main-sequence turn-off at B3 V, as well as a large number of supergiants with spectral types ranging from F to M. We use intermediate-resolution spectra of the evolved cool stars to derive their stellar parameters and find an essentially solar iron abundance. Under the plausible assumption that our photometry reaches stars still close to the zero-age main sequence, the cluster is located at $d \approx 5.5$ kpc and has an age of ∼60 Ma, though a slightly younger and more distant cluster cannot be ruled out. Despite the apparent good fit of isochrones, evolved stars seem to reside in positions of the colour–magnitude diagram far away from the locations where stellar tracks predict helium burning to occur. Of particular interest is the presence of four yellow supergiants, two on the ascending branch and two others close to or inside the instability strip.

Key words: stars: evolution – supergiants – open clusters and associations: individual: Berkeley 51.

1 INTRODUCTION

Evolved stars in open clusters represent the best test beds for theoretical evolutionary tracks. After the end of hydrogen burning in their cores, stars evolve towards lower effective temperatures, $T_{\rm eff}$, and become, according to their masses, red giants (RGs) or supergiants (RSGs). For a limited range of masses, loops in the HR diagram are expected to bring the stars back to the yellow supergiant region, where they can behave as classical Cepheids (e.g. Chiosi et al. 1992). As an example, in the most recent Geneva tracks (Ekström et al. 2012), stars of solar composition with masses between 5 and 9 $M_{\odot}$ experience these loops both for zero initial rotation and moderately high initial rotation, while older isochrones showed this behaviour at higher masses (Schaller et al. 1992). The exact mass range for which these loops happen depends on the physics of the stellar interior, generally modelled via poorly understood parameters (e.g. Chiosi et al. 1992; Mowlavi & Forestini 1994; Salasnich et al. 1999; Meynet & Maeder 2000). In particular, the extent of semi-convection and overshooting, which are not

⋆ E-mail: ignacio.negueruela@ua.es

well constrained, has crucial consequences on issues of fundamental importance in our understanding of Galactic chemical evolution, such as the ratio of initial mass to white dwarf mass (e.g. Jeffries 1997; Weidemann 2000) or the boundary between stars that leave white dwarfs as remnants and those that explode as supernovae (e.g. Poelarends et al. 2008).

Unfortunately, due to the rarity of high-mass stars and the short duration of the post-H-core-burning phase, most young open clusters are only moderately useful as test beds because of low number statistics (e.g. Ekström et al. 2013). For ages above 100 Ma, on the other hand, the number of RGs increases for a given cluster mass, meaning that several clusters are known to sport large populations of RGs (see Mermilliod et al. 2008). Finding young open clusters with large populations of evolved stars provides the laboratories that can help constrain the inputs of models and hence our understanding of stellar evolution (Negueruela 2016).

As part of such an endeavour, we have been searching through the data bases of poorly studied known open clusters to identify good candidates to massive young open clusters. Recent examples include the starburst cluster vandenBergh-Hagen 222, with a population of 13 yellow or red supergiants at an age ∼16–20 Ma (Marco et al. 2014), or the ∼50 Ma open cluster Berkeley 55, with six to seven

© 2018 The Author(s)
Published by Oxford University Press on behalf of the Royal Astronomical Society

Table 1. Log of the photometric observations taken at the NOT on 2010 June for Be 51. There are two observations for each exposure time.

Filter	Exposure times (s)	
	Long times	Short times
U	900	250
B	200	60
V	40	10

supergiants or bright giants (Negueruela & Marco 2012). Here we report on the identification of another faint, northern sky cluster as a young, massive cluster with a large population of evolved stars.

Berkeley 51 (Be 51) is a faint, compact cluster in the constellation Cygnus. The WEBDA data base[1] (Netopil et al. 2012) provides coordinates RA: $20^h11^m54^s$, Dec.: $+34° 24' 06''$ ($\ell = 72°.15$, $b = +0°.29$). Two previous estimates by Tadross (2008) and Kharchenko et al. (2013), based on existing photometric catalogues, agree on considering Be 51 an intermediate-age, distant cluster ($\tau = 150$ Ma, $d = 3.2$ kpc in Tadross 2008; $\tau = 180$ Ma, $d = 3.3$ kpc in Kharchenko et al. 2013, who estimate a reddening $A_V = 5.8$ mag). In contrast, a BVI CCD study by Subramaniam et al. (2010) concluded that it was an old ($\tau = 1$ Gyr) cluster at only $d = 1.3$ kpc, despite its high reddening of $E(B - V) = 1.6$. In this paper, we present a much more complete study of Be 51, including comprehensive spectroscopy, that reveals it as a distant, moderately massive young open cluster containing a large population of evolved stars.

2 OBSERVATIONS

2.1 Optical photometry

UBV photometry of Be 51 was obtained in service mode using Andalucía Faint Object Spectrograph and Camera (ALFOSC) on the Nordic Optical Telescope (NOT) at the Roque de los Muchachos Observatory (La Palma, Spain) on the night of 2008 September 19. In imaging mode, the camera covers a field of 6.5 arcmin × 6.5 arcmin and has a pixel scale of 0.19 arcsec pixel^{-1}.

Two standard fields from the list of Landolt (1992), MARK_A and PG 2213−006, were observed during the night in order to provide standard stars for the transformation. Since there is only one measurement of each field, we could not trace the extinction during the night, and so we used the median extinction coefficients for the observatory. The images were processed for bias and flat-fielding corrections with the standard procedures using the CCDPROC package in IRAF.[2] Aperture photometry using the PHOT package inside DAOPHOT (IRAF, DAOPHOT) was developed on these fields with the same aperture, 21 pixels, for each filter.

Images of Be 51 were taken in two series of different exposure times to obtain accurate photometry for a magnitude range. The log of observations is presented in Table 1. Photometry was obtained by point spread function (PSF) fitting using the DAOPHOT package (Stetson 1987) provided by IRAF. The apertures used are of the order of the full width at half-maximum (FWHM), 5 pixels for all images in the U and B filters and 4 pixels for the V filter images. We

---

[1] At http://webda.physics.muni.cz
[2] IRAF is distributed by the National Optical Astronomy Observatories, which are operated by the Association of Universities for Research in Astronomy, Inc., under cooperative agreement with the National Science Foundation.
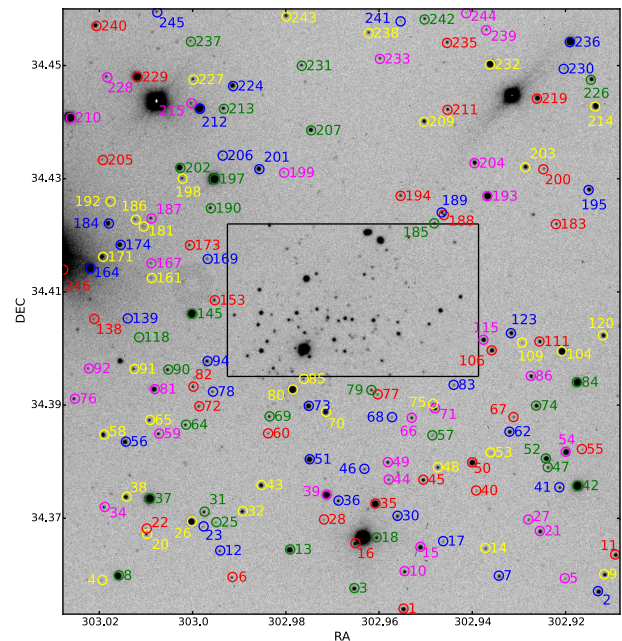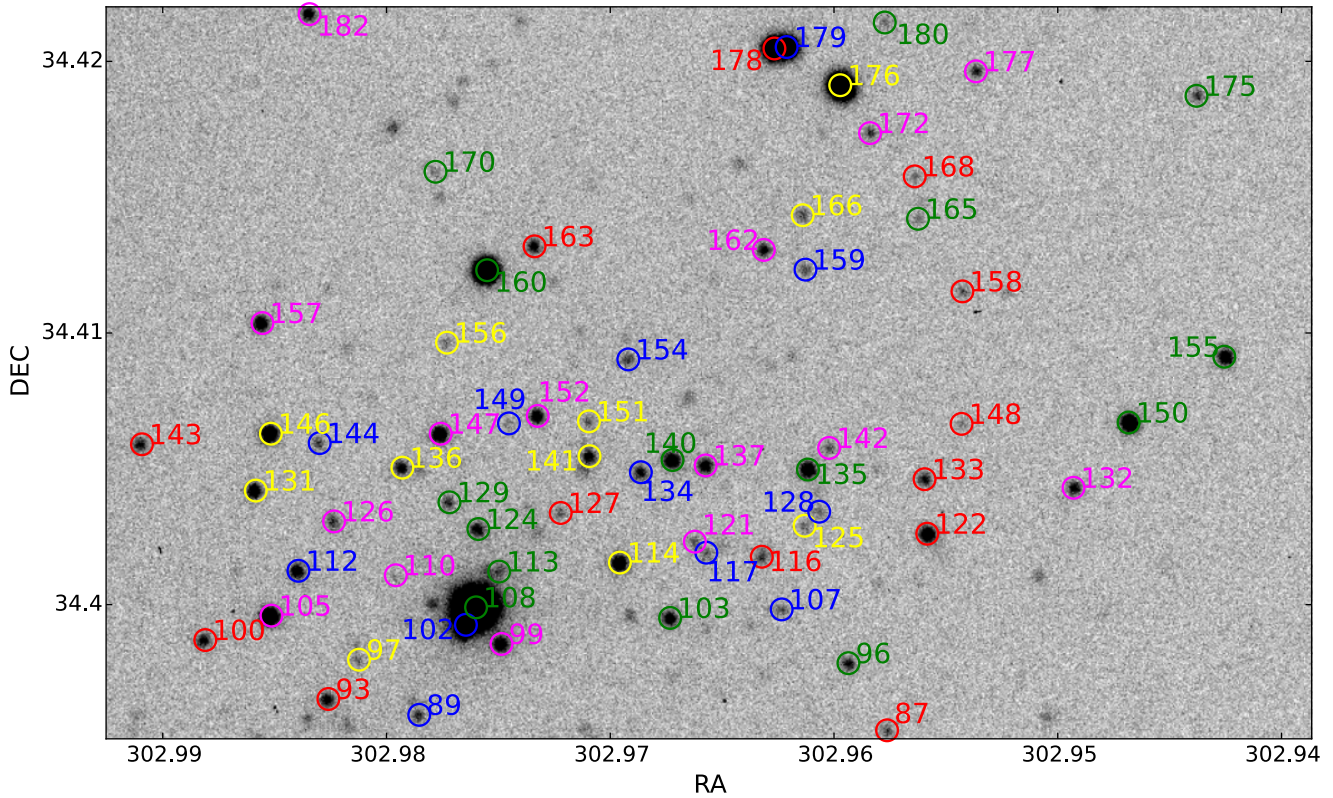

Figure 1. Finding chart for stars with photometry in the field of Be 51. The image is one of our deep *U*-band frames. Stars inside the rectangle (which approximately defines the cluster core) are marked in Fig. 2. Each star is identified by the nearest marker in the same colour as the circle around it (colours are assigned simply for visibility). The size of the image is the full FoV of ALFOSC.

selected ≈20 PSF stars in each frame, from which we determined an initial PSF, which we allowed to be variable (in order 2) across the frame. We then performed aperture correction to obtain instrumental magnitudes for all stars. Using the standard stars and the median extinction coefficients for the observatory, we carried out the transformation of the instrumental magnitudes to the standard system by means of the PHOTCAL package inside IRAF.

The number of stars that we could detect in all filters is limited by the long exposure time in the U filter. We identify all stars with good photometry in all three filters on the image in Figs 1 and 2. In Table B1, we list coordinates (obtained by a cross-match with 2MASS), their *UBV* photometry, and their 2MASS *JHK*$_S$ photometry, when available. The values of V, $(B - V)$, and $(U - B)$ are given together with the number of measurements and an error, which is the standard deviation of all the measurements whenever several measurements exist and the photometric error otherwise. The designation of each star is given by the number indicated on the images (Figs 1 and 2). We have three-band photometry for ∼250 stars in the field, but in the analysis we will only use 173 stars with photometric errors such that the error in their reddening-free Q parameter (see Section 3.3) is <0.07 mag (roughly corresponding to an uncertainty of one spectral type in photometric classification).

2.2 2MASS data

We obtained *JHK*$_S$ photometry from the 2MASS catalogue (Skrutskie et al. 2006). The completeness limit of this catalogue is set at $K_S = 14.2$. We selected only stars with 'good' quality flags in 2MASS (A or E), and photometric errors <0.05 mag in all bands. This leaves out many stars close to the centre of the cluster, where confusion becomes important at the spatial resolution of 2MASS.

We used the 2MASS data to carry out a preliminary selection of spectroscopic targets for an exploratory survey. We took a circle

Figure 2. Finding chart for stars with photometry in the central part of Be 51. Labelling as in Fig. 1.
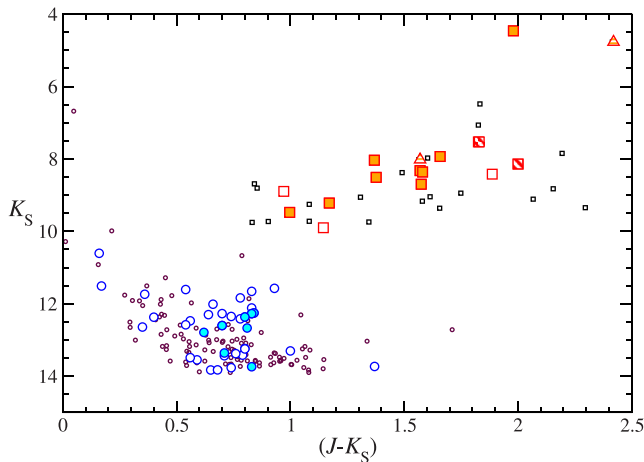

Figure 3. Colour–magnitude diagram for 2MASS data in circles of radius 3 arcmin (large symbols) and 7 arcmin (small symbols) around the position of Be 51. Circles represent objects selected as possible early-type stars, while squares are candidate luminous stars (selected as described in the main text). Filled symbols represent stars with spectra classified as likely members. Striped squares are stars with spectra that we do not consider as members. The triangles are more distant objects whose connection to the cluster is unclear.

of radius 3 arcmin around the nominal cluster centre and built the corresponding $K_S/(J - K_S)$ diagram (see Fig. 3). We cleaned the diagram by making use of the reddening-free Q_{IR} index, defined as $Q_{IR} = (J - H) - 1.8 \times (H - K_S)$. Early-type (OBA) stars are easily separated, as they display $Q_{IR} \approx 0.0$ (cf. Comerón & Pasquali 2005;

Negueruela & Schurch 2007). We selected stars with $-0.15 \leq Q_{IR} \leq 0.08$ (shown as large circles in Fig. 3). This range is intended to account for the typical errors in 2MASS (generally 0.03–0.05 mag in a given colour for stars with $K_S = 12$–13) and also include emission-line stars, which typically have $Q_{IR} \lesssim -0.05$ (e.g. Negueruela & Schurch 2007).

In addition, we selected bright stars with $K_S \leq 10.0$ and $0.1 \leq Q_{IR} \leq 0.4$, the range where Galactic red luminous stars are generally found (see Negueruela et al. 2012; González-Fernández et al. 2015, for a discussion of these criteria). These objects are displayed as big squares in Fig. 3. We then applied the same criteria to a circle of radius 7 arcmin around the nominal cluster centre (displayed as small symbols in Fig. 3). Comparison of both data sets shows a clear overdensity of bright stars in the central cluster area (almost half the bright stars in the large circle are inside the small circle, which has less than one fifth of the area). In addition, there is a strong overdensity of early-type stars with $K_S = 11$–13 in the central area, with most of them presenting $(J - K_S) \approx 0.75$. We interpreted this overdensity as the cluster main sequence (MS), and selected targets for the spectroscopy runs among these objects.

2.3 Spectroscopy

Spectroscopy of the brightest candidate members of Be 51 was obtained with the red arm of the Intermediate dispersion Spectrograph and Imaging System (ISIS) double-beam spectrograph, mounted on the 4.2 m William Herschel Telescope (WHT) in La Palma (Spain) in three separate runs. An initial survey was conducted with the R600R grating and the *Red+* CCD, a configuration that covers the 7600–9000 Å range in the unvignetted section of the CCD with a nominal dispersion of 0.5 Å pixel^{-1}. Data were taken during a

Table 2. Log of the WHT observations. The upper panel shows observations of cool luminous stars confirmed as members, all of which have been observed at least twice. The middle panel contains other cool luminous stars. The bottom panel includes candidate blue stars, observed only once.

Star	Exposure time (s)	Date (UT)	Counts per pixel[a]
126	30	21 Aug 2007	35 000
	350	28 Jun 2012	45 000
	200	2 Jul 2012	30 000
70	200	26 Jul 2007	24 000
	450	28 Jun 2012	10 000
134	200	26 Jul 2007	11 000
	400	2 Jul 2012	3000
301	200	26 Jul 2007	15 000
	500	28 Jun 2012	6000
172	200	26 Jul 2007	12 000
	350	2 Jul 2012	3000
162	200	26 Jul 2007	14 000
	600	2 Jul 2012	9000
302	200	26 Jul 2007	9000
	350	2 Jul 2012	2000
146	200	21 Aug 2007	16 000
	350	2 Jul 2012	3000
105	200	21 Aug 2007	15 000
	450	28 Jun 2012	4000
501	200	22 Aug 2007	18 000
502	400	22 Aug 2007	12 000
503	200	22 Aug 2007	15 000
	350	2 Jul 2012	4500
901	200	2 Jul 2012	9000
114	900	21 Aug 2007	7500
103	1200	22 Aug 2007	4000
122	900	21 Aug 2007	6000
150	1200	22 Aug 2007	13 000
143	900	21 Aug 2007	7000
147	900	21 Aug 2007	7000

Note. [a]Counts per pixel in the spectral direction after extraction of the whole slit width. Note that spectra from 2007 August were pre-binned by a factor of 2 to match the resolution element. For a correct estimation of the S/N, all the other spectra should have two pixels added.

service night on 2007 July 26 and then completed during a run on 2007 August 21. In July, the CCD was unbinned, and a 1.5 arcsec slit was used. In August, the CCD was binned by a factor of 2 in the spectral direction, and a 1.2 arcsec slit was used. For this grating and all slit widths >1.1 arcsec, the spectral resolution is oversampled, and the resolution element is expected to be ∼4 unbinned pixels. This has been checked by measuring the width of arc lines, which is on average ≈2.1 Å for both configurations. The resolving power of our spectra is therefore $R \sim 4200$.

The supergiants identified during this survey were then re-observed at higher resolution, using the R1200R grating in 2012 June and the unbinned *Red+* CCD. The nominal dispersion is 0.26 Å pixel^{-1}. We used a 0.9 arcsec slit that provides a resolving power of $R \sim 12\,000$. Unlike in the previous runs, each spectrum was taken together with an arc exposure at the same sky position, for accurate wavelength calibration. A log of all the WHT/ISIS observations is presented in Table 2. The average number of counts per pixel in the continuum around the Ca II triplet is given to estimate the signal-to-noise (S/N) ratio.

Candidate blue stars in Be 51, selected from our *UBV* photometry, were observed on the night of 2014 August 24 with the Optical System for Imaging and low-Intermediate-Resolution Integrated
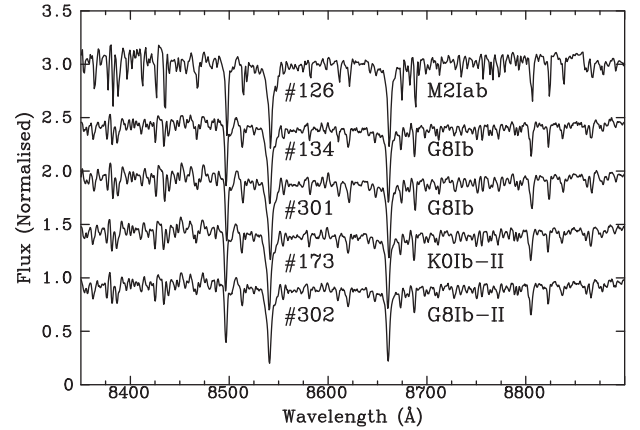

Figure 4. Intermediate-resolution spectra, taken with ISIS, in the region around the Ca II triplet of five bright red stars in the central concentration of Be 51.

Spectroscopy (OSIRIS) instrument, mounted on the 10.4 m Gran Telescopio Canarias (GTC) in La Palma (Spain). The instrument operated in the MOS mode, with 1.2 arcsec slitlets traced on a plate. The R2000B grism covers the nominal range 3950–5700 Å, but the actual spectral coverage for a given object is a strong function of its position on the plate. The nominal dispersion of the R2000B grism is 0.9 Å per binned pixel (the standard Marconi CCD42-82 mosaic is used in 2 × 2 binned mode). The resolving power, measured on arc lamp spectra, is $R \approx 1400$.

Only one plate was observed, as the effective field of 7.6 arcmin × 6.0 arcmin is much larger than the cluster size. Three 1895 s exposures were obtained. We reduced these data using the STARLINK (Currie et al. 2014) software packages CCDPACK (Draper et al. 2011) and FIGARO (Shortridge et al. 2014) by following standard procedures. The spectra have been normalized to the continuum using DIPSO (Howarth et al. 2014).

Finally, we observed one star (#126) with the High Efficiency and Resolution Mercator Echelle Spectrograph (HERMES), operated at the 1.2 m Mercator Telescope (La Palma, Spain) on 2011 June 15. HERMES reaches a resolving power $R = 85\,000$, and a spectral coverage from 377 to 900 nm, though some small gaps exist beyond 800 nm (Raskin & Van Winckel 2014). Data were homogeneously reduced using version 4.0 of the HermesDRS[3] automated data reduction pipeline, which provides order merged spectra. In this case, the target is very faint and there are essentially no counts shortwards of ∼5500 Å.

3 RESULTS

3.1 Spectral classification

Fig. 4 shows the spectra of five bright red stars in the field preselected as possible evolved members. Classification criteria for spectra at this resolution are discussed in Negueruela et al. (2012). The brightest star in the infrared, #126, is a luminous supergiant of spectral type M2 Iab. The four other stars are very similar to each other. They are all low-luminosity supergiants with spectral types close to K0 (see Table 3). We have at least two spectra for each star, and in all cases the spectra are consistent with the same classification.

[3] http://www.mercator.iac.es/instruments/hermes/drs

Table 3. Stellar parameters for cool stars in the field of Be 51. The top panel lists stars in the central condensation that are considered likely members. The bottom panel presents two other stars at higher distances.

Star	Spectral type	Date	$T_{\rm eff}$ (K)	$\log g$	[M/H] (dex)	ξ (km s^{-1})	MARCS grid	$v_{\rm hel}$ (km s^{-1})	$v_{\rm LSR}$ (km s^{-1})
126	M2 Iab	2012 Jun 28	3666 ± 39	0.0	0.23 ± 0.05	1.97	15 M$_\odot$	−13	−8
126		2012 Jul 2	3656 ± 40	0.0	0.23 ± 0.05	1.96	15 M$_\odot$	−10	−5
70	~F8 Ib	2012 Jun 28	–	–	–	–	–	−26	−21
134	G8 Ib	2012 Jul 2	4502 ± 102	1.0	0.04 ± 0.06	2.07	1 M$_\odot$	−7	−2
301	G8 Ib	2012 Jun 28	4560 ± 75	1.0	0.31 ± 0.04	2.14	1 M$_\odot$	−11	−6
172	K0 Ib-II	2012 Jul 2	4537 ± 95	1.0	0.16 ± 0.06	2.11	1 M$_\odot$	−24	−19
162	F8 Ib[a]	2012 Jul 2	6575 ± 65	1.5	0.14 ± 0.03	3.77	1 M$_\odot$	−11	−16
302	G8 Ib-II	2012 Jul 2	4432 ± 130	1.0	0.16 ± 0.06	1.99	1 M$_\odot$	−8	−3
146	F4 Ib	2012 Jul 2	–	–	–	–	–	−4	+1
105	F5 Ib	2012 Jun 28	6727 ± 103	2.0	0.14 ± 0.07	3.25	1 M$_\odot$	−9	−4
503	K2 Ib	2012 Jul 2	4275 ± 97	1.0	0.16 ± 0.05	1.8	1 M$_\odot$	−26	−22
901	M1 Iab	2012 Jul 2	3795 ± 52	0.0	0.05 ± 0.05	2.16	15 M$_\odot$	+1	+6

Note. [a]Spectral type in the spectrum analysed. It appears decidedly later in the lower resolution spectrum taken in 2007.
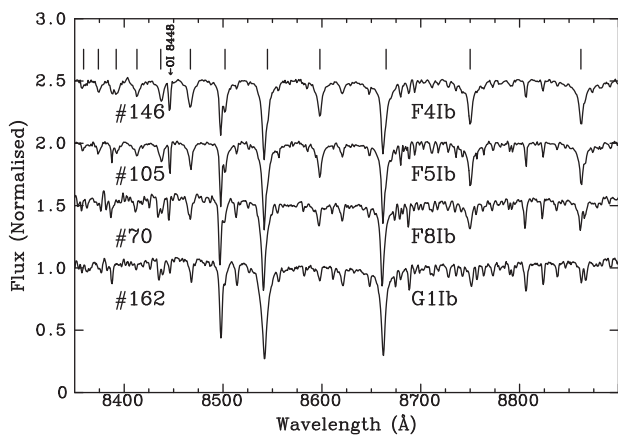

Figure 5. Intermediate-resolution spectra, taken with ISIS, in the region around the Ca II triplet of four bright yellow stars in the central concentration of Be 51. The vertical dashes indicate the positions of the Paschen lines, which weaken as we move along the spectral sequence (note that Pa 13, 15, and 16 blend with the stronger lines of the triplet). The O I 8448 Å line, also marked, shows a similar behaviour.

Fig. 5 shows the spectra of four candidate luminous stars with fainter K_S magnitudes and bluer colours. Comparison to MK standards observed at similar resolution (e.g. Cenarro et al. 2001) suggests that they are all F-type supergiants. This can be confirmed by measuring the strength of their Ca II triplet lines (e.g. Diaz et al. 1989; Mallik 1997). Two of the stars, #146 and #105, have very similar spectral types, even though they appear somewhat different because of different rotational velocity. They are mid-F supergiants. The other two stars present clear differences between the two spectra taken at different epochs. Star 70 is a late-F supergiant. Both spectra are close to F8 Ib, but the 2012 one looks discernibly earlier. In the case of #162, the differences are larger. It is F8 Ib in the 2012 spectrum, but clearly later (around G1 Ib) in the 2007 spectrum. As we will see in the following sections, both stars lie on positions compatible with the blue loop in the photometric diagrams.[4] The spectral types of all the cool stars are listed in Table 3. Note that two objects

---

[4] In a forthcoming paper, Lohr et al. (submitted) show that #162 is a 10 d Cepheid.

lack optical photometry and have been labelled as stars 301 (2MASS J20115344+3424427) and 302 (2MASS J20114858+3424420).

The GTC/OSIRIS observation provided classification spectra for 10 stars, which are listed in Table 4. Fig. 6 shows six of them. The S/N ratio varies greatly among them, but all allow spectral classification. We performed the classification via comparison to spectra of MK standard stars degraded to the same resolution. All the stars observed (corresponding to the top of the cluster blue sequence) are early- to mid-B stars. Due to high reddening, the S/N is quite low around Hγ and, when possible, we have used the set of metallic and He I lines in the 4 900–5100 Å range to improve the luminosity classification. The spectral types derived are listed in Table 4. The spectrum of star 143 shows very asymmetric Balmer lines, most likely indicating the presence of two stars (Fig. 6), one with spectral type ~B5 III and an earlier, less bright companion. The spectrum of #153 (not shown) is quite poor and seems to be blended with a late-type interloper (perhaps simply due to bad sky subtraction), but a ~B3 V classification is likely.

All the intrinsically blue stars that were observed in the Z band with the WHT were re-observed with GTC in the classification region, except for #103. For this object, we can derive an approximate spectral type B2 V from the WHT spectrum. This spectral classification is, however, much less accurate than those based on the blue spectral region, and this star will not be used to compare spectroscopic and photometric characteristics. One of the brightest candidates based on the 2MASS colours, star 150, turns out to be a low-luminosity A-type star, and therefore a foreground object.

3.2 Spectroscopic analysis

We used the higher resolution ISIS spectra of the cool stars to compute effective temperature ($T_{\rm eff}$) and iron abundance by comparing them to a previously generated grid of synthetic spectra. We employed the new version of the automated code STEPAR (see Tabernero et al. 2018), which relies upon spectral synthesis instead of equivalent widths (EWs) and uses a Markov chain Monte Carlo algorithm (EMCEE; see Foreman-Mackey et al. 2013) for optimization. We explored the parameter space using 20 Markov chains of 1250 points starting from an arbitrary point. As objective function, we used a χ-squared in order to fit any previously selected spectral features.

The synthetic spectra were generated using two sets of one-dimensional local thermodynamic equilibrium atmospheric models, based on 15 and 1 M$_\odot$ MARCS spherical atmospheric

Table 4. Intrinsic parameters for all very likely photometric members, ordered by dereddened magnitude. Spectral types are given for the 10 stars observed with GTC/OSIRIS and also for #103.

Star	Photometric spectral type[a]	Spectral type (if available)	$E(B-V)$
71	b3 iv		1.86
249	b3 iv		1.84
252	b3 iv		1.89
86	b6 iii		1.81
195	b6 iii		1.66
114	b3 iv	B3 III	1.76
147	b2v	B2 IVe	1.78[b]
131	b1v	B2 Ve	1.85[b]
175	b3 iv	B3 IV	2.02
143	b6 iii	B5 III	1.88
122	b3 iv	B3 III–IV	1.72
99	b2v		1.75
103	b3 v	B2 V[c]	1.79
137	b3 v	B3 IV–V	1.75
152	b3 v		1.73
267	b5 iv		1.76
141	b3 v		1.77
163	b3 v		1.77
44	b3 v		1.91
47	b5 v		1.78
185	b3 v		1.88
69	b5 v		1.72
93	b3 v		1.67
177	b5 v		1.75
153	b5 v	B3 V	1.73
82	b5 v	B5 III	1.72
154	b6 iv		1.77
79	b3 v		1.73
116	b3 v		1.72
269	b5 v		1.67
166	b5 v	B5 IV	1.73
169	b6 v		1.69

Notes. [a]Spectral types are derived from the photometry following the procedure described in the text, under the assumption of $\mu = 13.7$.
[b]Colour excess values for the confirmed Be star are not entirely interstellar.
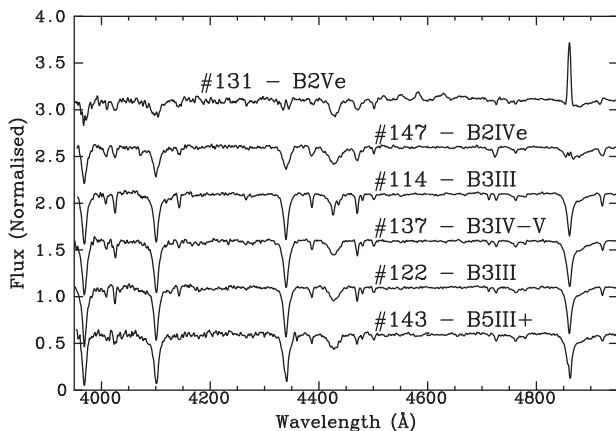[c]Derived from the *Z*-band spectrum, and so less certain.

Figure 6. GTC classification spectra of B-type stars in Be 51.

models (Gustafsson et al. 2008). The radiative transfer code employed was SPECTRUM (Gray & Corbally 1994). As line list, we employed a selection from the VALD data base (Piskunov et al. 1995; Kupka et al. 2000; Ryabchikova et al. 2015), taking into account all the relevant atomic and molecular features (dominated by TiO and CN) that can appear in cool luminous stars up to mid-M types. In addition, as Van der Waals damping prescription we employed the Anstee, Barklem, and O'Mara theory, when available in VALD (see Barklem et al. 2000). Effective temperature $T_{\rm eff}$ ranges from 4000 to 8000 K with a step of 250 K for the spectra generated using $1\,M_\odot$ atmospheric models. For the $15\,M_\odot$ MARCS synthetic models, $T_{\rm eff}$ varies from 3300 to 4500 K; the step is 250 K above 4000 and 100 K otherwise. Finally, the metallicity ranges from $[M/H] = -1.0$ to 1.0 dex in 0.25 dex steps for $1\,M_\odot$ models, whereas $15\,M_\odot$ MARCS models cover only from $[M/H] = -1.0$ to 0.5 dex, in 0.25 dex increments. Surface gravity ($\log g$) varies from -0.5 to 2.0 dex in 0.5 dex steps, when available in each MARCS grid. We convolved our grid of synthetic spectra with a Gaussian kernel (FWHM $\approx 30\,{\rm km\,s^{-1}}$) to account for the instrumental broadening.

The present version of STEPAR allows the derivations of any set of stellar atmospheric parameters simultaneously. In this case, we restricted them to only two variables, $T_{\rm eff}$ and metallicity ($[M/H]$). Given the strong degeneracy between $\log g$ and metallicity, surface gravity was kept fixed to values compatible with the position of stars in the observational HR diagram (see Section 4.2 and compare to Table 3); microturbulence (ξ) was adjusted according to the 3D model-based calibration described in Dutra-Ferreira et al. (2016). Since our stars are more luminous than any of their calibration benchmarks, we have checked the consistency of our results by obtaining parameters with ξ fixed to 3 and $5\,{\rm km\,s^{-1}}$ (i.e. higher than any value used) for all stars. The derived $T_{\rm eff}$'s are quite similar in all cases. Increasing ξ has some effect on the metallicity derived (higher ξ implies lower $[M/H]$), but even for the extreme case it is less than ~ 0.2 dex. Our analysis employs some empirically selected lines of Mg, Si, Ti, and Fe (Dorda et al. 2016) in the spectral range around the CaT, 8400–8900 Å. The results of the analysis are listed in Table 3.

The spectrum of star 70 cannot be properly fitted. The Fourier transform indicates two components separated in velocity. Analysis of the spectrum reveals two similar objects separated by about $25\,{\rm km\,s^{-1}}$, i.e. barely resolved at our resolution. This multiplicity could explain the mild spectral variability. Star 146 cannot be fitted either; it is probably too hot for the set of lines used, more suited for K/M spectral types, but fast rotation also helps to dilute the diagnostic lines. We can estimate its rotational velocity even if the resolution of our spectrum is quite low for this task. As we have a good idea of the physical parameters of the star, which must be quite similar to those of star 105, we can choose a suitable stellar model from the POLLUX data base (Palacios et al. 2010) and convolve it with a Gaussian of width appropriate to our spectral resolution. We can then take this synthetic spectrum and convolve it with a rotation profile following Gray & Corbally (2009), and compare the result for different values of $v_{\rm rot}$ and limb darkening with our spectrum. This was done following a Bayesian framework, so that we could marginalize over the limb darkening parameter, arriving at a value $v_{\rm rot} = 53.2 \pm 1.5\,{\rm km\,s^{-1}}$. This is a very high rotational speed for a supergiant, but we do not see any evidence for a second component in the spectrum.

For all the other stars, we obtain a convincing fit. Due to the low number of lines used in the analysis, the formal uncertainties are moderately large. The values of $T_{\rm eff}$ found, though, are appropriate for the observed spectral types. Likewise, the analysis of the two

spectra of star 126 shows rather better agreement than indicated by the formal uncertainties. Although some of our metallicity determinations have moderate uncertainties, the seven likely members in the cluster core present consistent values. If we average them using the S/N of the spectra as weight, we obtain a mean of $+0.17 \pm 0.09$ dex, slightly supersolar. This result implies that we can safely use solar-metallicity isochrones for the analysis.

3.3 Observational HR diagram

We start the photometric analysis by plotting the $V/(B - V)$ and $V/(U - B)$ diagrams for all stars in the field. In Fig. 7, we can observe that the cluster sequence (as defined by the spectroscopically identified early-B stars) is heavily contaminated by what seems to be foreground population. All the confirmed B-type stars have $(B - V) \approx 1.5$, and therefore we can assume that this is the location of the cluster sequence. We proceed with a classical photometric analysis, following Johnson & Morgan (1953) and Johnson (1958).

For early-type stars, it is possible to achieve approximate classification by means of the reddening-free Q parameter, defined as

$$Q = (U - B) - \frac{E(U - B)}{E(B - V)}(B - V), \qquad (1)$$

where $\frac{E(U-B)}{E(B-V)}$ depends on the extinction law (taking a standard value of 0.72; Johnson & Morgan 1953) and also weakly on the spectral type. For a standard extinction law, we can use the expression

$$\frac{E(U - B)}{E(B - V)} = X + 0.05 E(B - V), \qquad (2)$$

where X depends weakly on spectral type (or, correspondingly, intrinsic colour; Johnson 1958), to calculate an accurate Q parameter. Since there are 10 early-type members for which we have both classification spectra and *UBV* photometry (see Table 4), we can use them to check if this is a valid approximation. From the spectra, we find that star 131 is a Be star with heavy veiling and anomalous colours, which can thus not be used for this purpose. Star 147 has weak Be characteristics, but still can be left out. For the other eight stars, we calculated $E(U - B)$ and $E(B - V)$ using the intrinsic colours of Fitzgerald (1970). The average of the reddening slope for them is 0.73 ± 0.04, with the error reflecting the standard deviation. On the other hand, using equation (2) with the value listed for a typical spectral type B3 in Johnson (1958), we find a slope of 0.74. This confirms that the extinction in this direction is standard (see also Section 4.1 later) and that we can use Q with this value of the slope.

Now we use the expression $(B - V)_0 = 0.332 \cdot Q$ (Johnson 1958) to estimate the intrinsic colours and hence the colour excess $E(B - V)$ to each star. For the stars with spectra, we can compare the values of $(B - V)_0$ obtained from the spectral type calibration with those derived from the Q method. The average difference is -0.01 ± 0.01 mag, and all the differences are within the typical dispersion of the calibration. The photometric classifications agree with our spectra in placing the MS turn-off at B3.

Application of this method reveals that a large fraction of the stars in our photometry are B-type stars (i.e. $Q < 0$). However, many of them have to be foreground to the cluster. For example, star 42 has $Q = -0.61$, corresponding to a mid-B star, but with $V = 14.3$ and $(B - V) = 0.79$, it is very far away from the position of the spectroscopic members. In addition, there is a significant fraction of late-B stars $(0 > Q > -0.2)$ that have $(B - V) \lesssim 1.1$. These objects are in all likelihood foreground interlopers. This high percentage of early-type contaminants is not so surprising as one could naïvely

think, because the line of sight goes through the Galactic plane, reaching a high distance, and we are selecting only objects with good *U*-band photometry. To confirm this foreground character, we divided the B-type stars into two groups, those with $E(B - V) > 1.3$ and those with $E(B - V) \leq 1.3$. The former group contains most of the stars with spectral types B3–B5 and is much more tightly concentrated around the position of the cluster than the latter. So we can start our membership determination by discarding stars with values below this threshold as non-members.

The eight non-emission stars with classification spectra (which had been selected because they seemed to belong to the top of the cluster sequence) have an average $E(B - V) = 1.80$ with a standard deviation $\sigma = 0.10$. The standard deviation indicates that the colour excess is only moderately variable for all these likely members. In view of this, we can increase our threshold by rejecting stars with $E(B - V)$ more than 3σ away from this value as probable non-members. There are no stars with colour excesses more than 2σ above this average, but many objects with values lower than 3σ below the average.

To make the final selection, we proceed with an iterative approach. First, we divide the sample into two groups. Stars with $E(B - V) \geq 1.65$ (less than 1.5σ away from the average for stars with spectra) are taken as likely members, while the rest are taken a possible members. For the first list, we derive photometric spectral types by comparing their Q values to the calibration of Johnson (1958) for MS stars. We then calculate a first estimate of the extinction by taking the intrinsic colours from Fitzgerald (1970) corresponding to this photometric type, calculating the corresponding colour excess and then applying $A_V = 3.1 \times E(B - V)$. With this value, we deredden all the stars and obtain a dereddened magnitude $m_V = V - A_V$.

For the second list (stars with $1.47 \leq E(B - V) < 1.65$), we carry out the same procedure separately. We then plot the likely members and the possible members against the observational zero-age main sequence (ZAMS) from Schmidt-Kaler (Aller et al. 1982) displaced at different distance moduli (as in Fig. 8). We obtain an initial cluster distance modulus (μ). After subtracting this μ, we compare the absolute magnitude of each star to the photometric spectral type to estimate whether the star has to be a giant or a dwarf to belong to the cluster. Taking into account this luminosity classification, we then proceed to re-estimate the spectral type for the objects that must be giants to be cluster members, using the corresponding Q calibration from Johnson (1958). The colour excesses are re-calculated and the process converges, because the differences in colour between giants and MS stars are very small. We then re-check the fit to the ZAMS and proceed to reject as non-members objects that should have spectral types unexpected for a cluster with a turn-off at B3 (for example, b8 iv) if they were at the cluster distance. A few objects with spectral type b7 that are too bright to be on the MS are moved from the list of likely members to the list of possible members. This does not affect our ZAMS fit, which steadily returns $\mu = 13.7$. Fig. 8 (top panel) shows the fit of the ZAMS to the very likely and possible members that remain after this procedure. The turn-off around $(B - V)_0 \approx -0.20$ seems to be well defined. The two detected Be stars fall clearly to the left of this turn-off, but this is not unusual for Be stars (and their spectral types show them to be blue stragglers in any case). A third star, #99, for which we have no spectrum, occupies a similar location, and could also be a Be star.

The fit is only moderately satisfactory, but as illustrated by the other two values of μ shown, is the best possible. Unfortunately, the position of the ZAMS seems to be determined mainly by stars in the list of possible members. This introduces the doubt of whether our
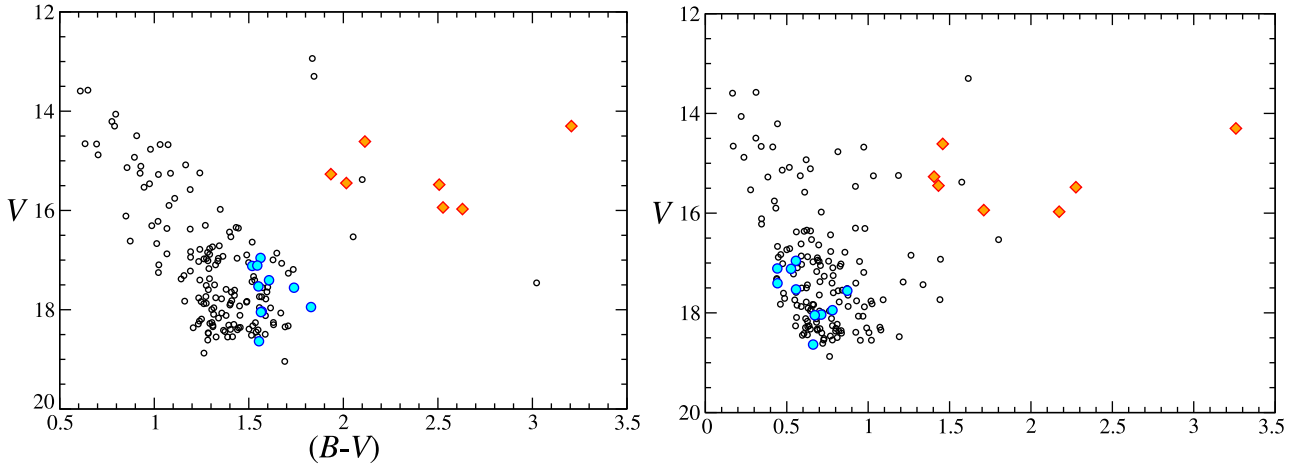
Figure 7. Raw CMDs for Be 51, from our *UBV* photometry. The location of the stars observed with GTC and confirmed as early B-type stars is marked by the filled circles. The location of stars observed with the WHT and confirmed as cool supergiants is shown with filled diamonds.
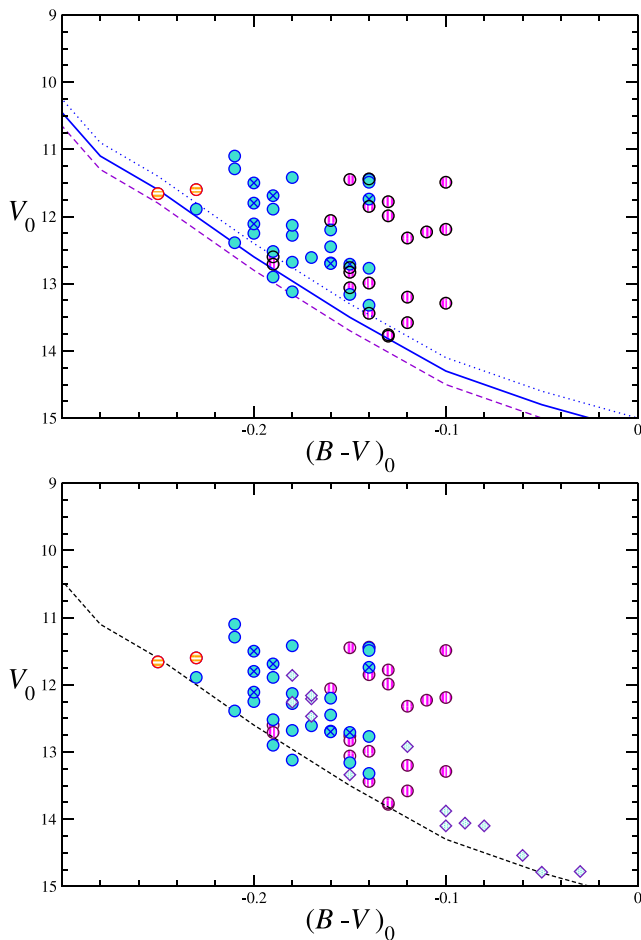

Figure 8. Top panel: dereddened CMD for very likely (filled blue circles) and possible (magenta circles with vertical stripes) members of Be 51 with the ZAMS of Schmidt-Kaler displaced at different distance moduli ($\mu = 13.5$, 13.7, and 13.9). The two Be stars are marked by orange circles with horizontal stripes. Bottom panel: the same with the confirmed members of Melotte 20 displaced to the same μ overplotted as cyan diamonds.

photometry is really reaching deep enough to touch the ZAMS. On the one hand, since stars with types B5–6 V are much fainter than the B3 V and B5 III objects that we have observed spectroscopically and our photometry is not very deep, it makes sense to assume that we reach only those ZAMS members with rather lower than average reddening (that have thus been included in the list of possible members). On the other hand, the luminosity classes derived from the spectra are consistently lower than those implied from the photometric types at $\mu = 13.7$. In fact, if we assume $A_V = 3.1 \times E(B - V)$ and the intrinsic magnitude calibration of Turner ([1980](#)) to derive spectroscopic distances for the blue stars with spectroscopy, we obtain an average $\mu = 14.4 \pm 0.5$, leaving aside again stars 131 and 143. The two values are just compatible within their respective errors (in view of the top panel of Fig. [8](#), a conservative error of ± 0.2 mag is assumed for the visual fit of the ZAMS as a lower envelope, given the uncertainties under discussion), but the difference is quite significant.

To investigate this issue further, in the lower panel of Fig. [8](#), we have added the members of Melotte 20 (the α Per cluster), a very well studied cluster that also has an MS turn-off at B3 V. Taking the photometry from Harris ([1956](#)), we have displaced them from their *Hipparcos* μ of 6.2 mag (van Leeuwen [2009](#)) to $\mu = 13.7$ by applying exactly the same dereddening procedure. We notice that the B3–5 V stars in Mel 20 (including the MK primary B3 V standard 29 Per) are well separated from the ZAMS, while in Be 51 we have B3 V stars all the way down to the ZAMS. This implies that Be 51 is somewhat younger than Mel 20. The confirmed late-B members of Mel 20 trace very well the ZAMS, giving further support to the value that we take as definitive $\mu = 13.7 \pm 0.2$, corresponding to $d = 5.5 \pm 0.5$ kpc.

Leaving out the two known Be stars, the average reddening for stars in the list of very likely members is $\langle E(B - V) = 1.78 \rangle$ with a 1σ dispersion of 0.08 mag. This is essentially identical to the values obtained for the spectroscopic members alone, thus confirming the validity of the selection criteria. The objects in this list fulfil all the requisites to be cluster members. Their derived properties are listed in Table [4](#). The list of possible members, given in Table [5](#), includes two b3 v stars that fall together with the very likely members. The membership of these two objects is rather likely, as B3 field stars are rare, and thus suggests that some stars with lower reddening do indeed belong to the cluster population. On the other hand, a number of objects with classifications b5–7 iii that are fainter than

Table 5. Intrinsic parameters for stars that could be members, ordered by dereddened magnitude.

Star	Spectral type[a]	$E(B-V)$
174	b6 iii	1.59
56	b5 iii	1.58
30	b7 iii	1.84
184	b7 iii	1.53
21	b6 iii	1.63
9	b7 iii	1.63
2	b5 iii	1.50
246	b7 iii	1.54
31	b7 iii	1.71
48	b7 iii	1.69
239	b7 iv	1.77
111	b3 v	1.62
248	b3 v	1.61
136	b5 v	1.64
102	b5 v	1.53
100	b6 v	1.59
49	b5 v	1.55
85	b7 iv	1.71
144	b7 iv	1.65
20	b5 v	1.57
14	b7 v	1.56
72	b7 v	1.50
91	b7 v	1.50

*Note. [a]*Spectral types are derived from the photometry following the procedure described in the text. The luminosity class indicated is that needed to be a cluster member, but not necessarily the true value.

the B3 III–IV stars are most likely interlopers. In any event, we must take into account that errors in Q are $\gtrsim 0.05$ mag for the fainter cluster members, and this can imply changes by almost one whole subtype, which could move an object from one list to the other.

4 DISCUSSION

4.1 Extinction

Cluster members with spectroscopy give an average $\langle E(B-V)\rangle = 1.80 \pm 0.10$. There is a degree of variability in extinction, expected for a distant object in this region of the Galactic plane. Images of the area (e.g. DSS2) reveal the presence of extended nebulosity in this area, and a possible uncatalogued H II region about 6 arcmin NE from the cluster. *WISE* images also show substantial dust emission over the whole area. In the optical images, there is a clear contrast between the high stellar density seen to the east and south of the cluster and the much lower density to the west and north-west, suggestive of a foreground dark cloud. The objects listed in Table 4 display a moderately broad range of colour excesses, but this is by design (a consequence of the selection procedure in Section 3.3), and so this range should be taken as a lower limit. The list of possible members in Table 5 includes two b3 v stars (#111 and #248) that are very likely to belong to the cluster and present $E(B-V) \approx 1.6$, significantly below the range used to define certain members. On the other hand, a number of objects in Table 5 with classifications b5–7 iii that are less bright than the stars around the turn-off are unlikely to be members, even though some of them have $E(B-V) > 1.7$. This confirms that $E(B-V)$ alone is not enough to identify members,

while the range of $E(B-V)$ present in the cluster is likely wider than that adopted to select certain members.

To verify that the reddening law can be approximated by the standard values, we can also calculate the infrared excess for very likely members, using the calibration of intrinsic colours of Winkler (1997), the photometric spectral types, and $(J-K_S)$ values from 2MASS. We find $\langle E(J-K_S)\rangle = 0.89 \pm 0.06$, in line with the dispersion expected from the optical value (taking into account the relatively large errors of 2MASS for the faintest objects). We find

$$\frac{\langle E(J-K_S)\rangle}{\langle E(B-V)\rangle} = 0.50, \tag{3}$$

in good agreement with the expectations for a standard extinction law. As the two averages are obtained with different samples,[5] the average of the ratios $E(J-K_S)/E(B-V)$ for individual targets with good-quality photometry, namely 0.49 ± 0.03 (where the error is the standard deviation), is probably more informative, and again ratifies the standard reddening law.[6]

Despite this, an attempt to individually deredden members with good 2MASS photometry using the intrinsic colours of Winkler (1997) results in positions on the colour–magnitude diagram (CMD) that are too red compared to the isochrone. As this situation has prevented us from individual dereddening of stars in the past (e.g. Marco et al. 2014), we have carried out an analysis of the infrared reddening law for the field. For this purpose, we take all the stars that had been selected in Section 2.2 as likely early-type stars with good-quality 2MASS photometry within the central 3 arcmin and plot their $(J-H)$ and $(H-K_S)$ colours, together with the reddening vector, compared to the expected position of early-type stars according to several references in Fig. 9. As can be seen, the observed position of all the stars lies along the standard reddening vector. It is clear that all stars deproject to positions compatible with the observational colour calibration of Winkler (1997), even though they are in the *JHK* system and some small differences with the 2MASS system are expectable, but not with the theoretical positions predicted by either the Geneva or Padova isochrones, which are in the 2MASS system. We have repeated this experiment with the much younger open cluster Berkeley 90, which shows strong differential reddening (Maíz Apellániz et al. 2015), coming to an identical conclusion: in the near-infrared (near-IR) colour–colour diagram, early-type stars project along the reddening line to a locus compatible with the empirical colours of B-type star, but not with the colours found in the isochrones. This suggests that the transformations used to convert the isochrones from the theoretical plane to magnitudes and colours do not reproduce well the near-IR photometry of early-type stars. Note that the issue does not concern the $(J-K_S)_0$ colour, which is quite well reproduced (as can be seen in Fig. 11), but the $(J-H)_0$ and $(H-K_S)_0$ colours. The first is always too high and the second always too low.

4.2 Cluster parameters

Using the values from the previous analysis, we plot a dereddened CMD for the cluster in Fig. 10. The supergiants have been dereddened following the procedure of Fernie (1963), which transforms the observed $E(B-V)$ to an equivalent $E(B-V)$ for early-type

---

[5] Because not all our photometric members have 2MASS photometry passing the quality criteria.

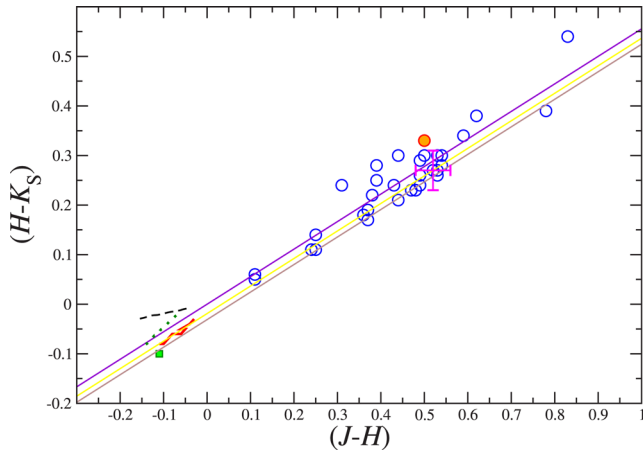[6] A value of 0.52 is expected for Rieke & Lebofsky (1985).

Figure 9. Colour–colour diagram for early-type stars in the central 3 arcmin of the field, selected as in Section 2.2. The thin straight lines are reddening vectors for a standard Rieke & Lebofsky (1985) extinction law that go through the position of three spectroscopically confirmed cluster members. The thick (red) wavy track is the locus of luminosity-class V B-type stars according to the observational calibration of Winkler (1997). The dotted line is the position of stars with masses between 3 and $12 \, M_\odot$ in a PARSEC (Bressan et al. 2012) 3 Ma isochrone (essentially, a ZAMS for B-type stars). The dashed line is the corresponding position for $3–12 \, M_\odot$ in a 3 Ma Geneva (Georgy et al. 2013) isochrone. The green square is the colour of all O-type MS stars according to the synthetic models of Martins & Plez (2006). The orange circle is the Be star 147. The error bars indicate the typical uncertainty in the photometry.

Figure 11. Dereddened CMD diagram for very likely members with useful 2MASS photometry. The isochrones are as in Fig. 10.

be constrained with the observed CMD. While the position of the supergiants narrows down significantly the range of possible ages, isochrones with high initial average rotations are almost indistinguishable from younger isochrones with lower initial rotation. For example, isochrones for 30 Ma with no rotation and 40 Ma with a moderately high rotation ($\Omega/\Omega_{crit} = 0.5$) are almost identical. As a compromise, we will use isochrones with moderate rotation, $\Omega/\Omega_{crit} = 0.3$.

If we accept the value of $\mu = 13.7$ that we obtained from the ZAMS fitting, then the isochrone for 60 Ma provides a good fit to the data. If, however, we accept the $\mu = 14.4$ that we obtain from the spectral classification, and thus the implication that our photometry might not be deep enough to reach the ZAMS, then the isochrone for 40 Ma provides a similarly good fit. The position of the RSGs around $(B - V)_0 = 1.1$ may be considered as support for the older value, but we must note that the good agreement with the isochrones must be interpreted with great caution. The evolved stars occupy positions compatible with the isochrones, but not those where the models predict that they should spend most of the time. To illustrate this, we have generated an artificial cluster using the interactive tools made available by the Geneva group[8] (Georgy & Ekström 2017) and employing the same astrophysical parameters that we use in the fit: $\Omega/\Omega_{crit} = 0.3$, solar composition, and $\tau = 60$ Ma. The cluster initially has 20 000 intermediate-mass stars, so that statistical sampling is not an issue. This artificial cluster is overplotted in Fig. 10, displaying the main properties of the evolutionary tracks: stars spend the first part of the He-burning phase as rather cool red giants (with spectral types K4–M0) and the second half as blue (A or F) supergiants. None of the evolved stars occupy the regions of highest density in the synthetic cluster. In particular, the model predicts that $\gtrsim$30 per cent of the He-burning stars should appear as post-RSG A-type supergiants, while we do not see any.

This discrepancy is not unique to Be 51, but widespread. The similarly aged cluster Berkeley 55 contains one late-F and five K (super)giants. Except for one, the spectral types of the K super(giants) place them at the same position on the isochrone as the Be 51 objects (Negueruela & Marco 2012). There are other well-studied clusters with similar ages, but they do not contain many evolved stars. For example, IC 4665 has no evolved stars, while Melotte 20 only includes the F5 Ib supergiant α Per. Looking at

Figure 10. Dereddened CMD for very likely members (blue filled circles and diamonds) and possible members (brown striped circles) of Be 51. The solid blue line is the 40 Ma Geneva (Georgy et al. 2013) track displaced to the spectroscopic $\mu = 14.4$. The dash–dotted green line is the 60 Ma Geneva track displaced to $\mu = 13.7$. The dashed red line is the 65 Ma PARSEC (Bressan et al. 2012) isochrone displaced to $\mu = 13.7$. The grey points are stars from the synthetic cluster mentioned in the text, generated with the best-fitting parameters and the tools of the Geneva group.

stars to account for colour effects.[7] To determine cluster parameters, we used the isochrones of Georgy et al. (2013) that cover the B-type range at a wide range of initial rotational velocities, v_{rot}. The effects of rotation introduce an extra dimension that cannot

---

[7] This procedure results in $\langle E(B - V) \rangle = 1.76 \pm 0.12$ for seven supergiants with photometry, in perfect agreement with the values for the blue members.
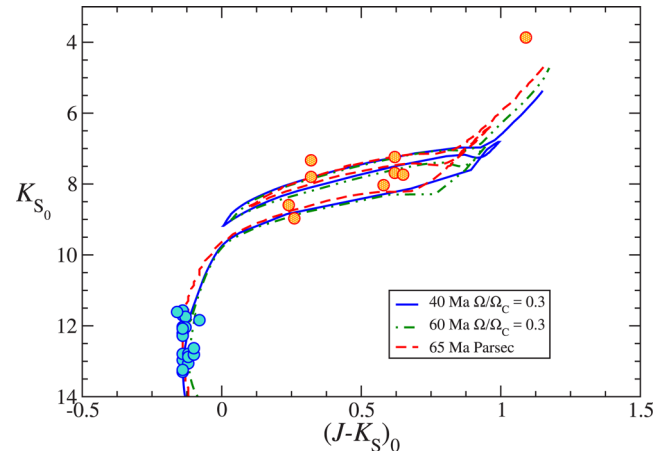
[8] https://obswww.unige.ch/Recherche/evoldb/index/

the literature, we find NGC 4609, NGC 6546, and Trumpler 3 with one red (super)giant each; NGC 6520 and NGC 6649 contain both F-type and red (super)giants, while NGC 6834 and NGC 7654 contain one F supergiant each. Only two clusters of similar age, NGC 5281 and NGC 2345, have known A Ib/II stars, but their locations on CMDs are compatible with stars moving off the MS, not with post-RSG nature. Even when we add together all these clusters, the total population is still small. However, the fraction of F-type stars is much higher than predicted by the Geneva models, while post-RSG A supergiants are almost absent. This suggests that the models predict a blue loop that extends to higher temperatures than supported by observations. In fact, if we plot a 65 Ma PARSEC isochrone (Bressan et al. 2012) in Fig. 10, we see that the only significant difference with the 60 Ma moderate-rotation Geneva isochrone is the size of the blue loop, which seems more compatible with the observations. Even then, the two mid-F supergiants in Be 51 occupy positions more consistent with the 'Hertzsprung gap' than with the loop.

As a further test, in Fig. 11 we plot the individually dereddened 2MASS data for the supergiants and the few blue members with high-quality photometric values together with the same isochrones used to fit the optical data. For the cool supergiants, we use the average calibration of González-Fernández & Negueruela (2012) for K and M stars, and the intrinsic colours of F-type supergiants from Koornneef (1983) transformed to the 2MASS system according to the equations of Carpenter (2001).[9] The match is quite good, but we note the following.

(i) The RSGs lie very far away from their expected position. However, this is likely an artefact of the intrinsic colour calibration, which goes from $(J - K_S)_0 = 0.58$ at G8 I to $(J - K_S)_0 = 0.87$ at K1 I (while it is 1.05 at M1 I).

(ii) The position of star 70 is slightly different from its location in the optical diagram. However, this is entirely dependent on the assumption of an F8 Ib spectral type. The $(B - V) = 2.52$ of #162 is much redder than the $(B - V) = 2.11$ of #70, but both have the same $(J - K_S) = 1.37$. With a spectral type F8 Ib, #70 has an $E(J - K_S) = 1.04$, well above the cluster average. All this suggests that #70 may have had a later spectral type at the time of the 2MASS observations.

(iii) The position of star 126 is completely inconsistent with the rest of the cluster in both diagrams.

We cannot give too much weight to the position of any of the individual evolved stars, as post-MS evolution is fast, and stochastic effects must contribute strongly to the very different evolved populations seen in the clusters mentioned above. To quantify this effect, 100 synthetic clusters were generated, all with the same parameters: solar metallicity, an age of 60 Ma, and a distribution of initial rotational velocities. Each cluster has an initial total mass around 3000 M$_\odot$, i.e. typical for a moderately massive Galactic young cluster. Details of the clusters are presented in Appendix A. The number of supergiants in a given cluster ranges from zero (7 out of 100 clusters) to six (5 out of 100 clusters). The distribution is shown in Fig. 12. Most clusters have between two and four evolved stars (about 20 per cent in each case), and the average number is three supergiants per cluster. This suggests that Be 51 must have a higher initial mass, at least twice as much to be in the range of
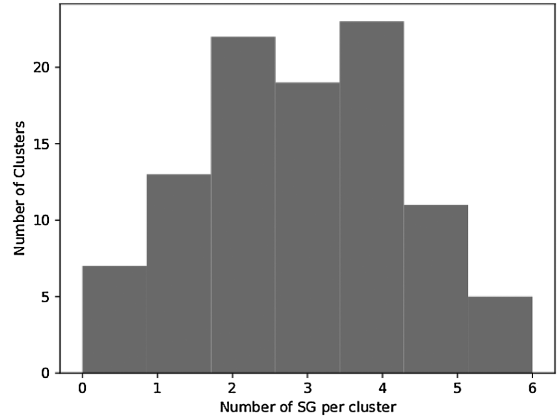
Figure 12. Number of supergiants found in a sample of 100 synthetic clusters with masses ~3000 M$_\odot$. The plot shows the number of clusters containing a given number of supergiants (see Appendix A).

statistical probability and most likely three times more, i.e. between 6 and 9×10^3 M$_\odot$.

4.3 Radial velocities

Radial velocities were calculated following the procedure outlined in Koposov et al. (2011). Since ISIS is attached to the Cassegrain focus of the WHT, it moves with the telescope, and is subject to large flexures. The method employed uses sky emission to refine possible systematics remaining in the wavelength calibration, so that all the spectra are in a common system that can then be anchored by using velocity standards. After this, it compares the observed spectra with a battery of models using a Bayesian framework. This has the advantage that it is possible to marginalize over any parameter in which we are not interested, removing it from the analysis while at the same time taking it into account when deriving uncertainties. In our case, we marginalize over the continuum normalization, since continuum determination is almost impossible at these resolutions for late-type stars, and over the stellar model, so that the derived velocities are not model dependent. According to the ISIS manual, an internal accuracy of 2 km s^{-1} can be achieved with R1200R, though a small systematic shift could be present. Two observations of star 126 taken on two separate nights (four nights apart) differ by 3 km s^{-1}, suggesting that the manual does not overestimate greatly the accuracy achievable. The accuracy is likely to be lower for the F-type stars, which have less (and generally broader) lines in the range used. The radial velocities measured are listed in Table 3.

At first sight, the radial velocities do not seem consistent with a single population. The average of all the values (including the two measurements of #126) is $v_{LSR} = -8$ km s^{-1}, with a standard deviation of 5 km s^{-1}. However, we can see that there are only three stars with velocities moderately different from the rest. Of these, two are the objects identified as spectroscopic variable, stars 70 and 162. If these objects are on the instability strip or binary (as seems to be the case of #70), radial velocity variations are expected. If we leave out these two stars, there is only one outlier, #172. This object could be in a binary or perhaps has recently been ejected from the cluster. If we also ignore it, the other six objects give an average of $v_{LSR} = -4$ km s^{-1}, with a standard deviation of 2 km s^{-1}, perfectly compatible with the expected internal accuracy of the measurements.

We calculated the Galactic rotation curve with respect to the local standard of rest (LSR) in the direction of Be 51 using the fit of Reid

---

et al. (2014), with $R_0 = 8.34$ kpc and $\phi_0 = 252.2$ km s^{-1}. A cluster velocity of $v_{LSR} = -4$ km s^{-1} corresponds to a kinetic distance of ≈ 5.5 kpc, in very good agreement with the photometric distance. A longer distance of 7.5 kpc would correspond to a radial velocity $v_{LSR} \approx -25$ km s^{-1}. Therefore, the observed radial velocity favours the distance derived from the photometric solution. At a distance of ~ 5.5 kpc and with $\ell \approx 72°$, Be 51 would be placed behind the whole extent of the Local arm, which explains its high and patchy extinction. Xu et al. (2013) show that the Local arm is a major structure, consisting of several important star-forming regions and extending until at least 4 kpc away from the Sun in this direction. However, at this distance Be 51 would already be in the Perseus arm. Indeed, for a distance $\gtrsim 6.5$ kpc, Galactic structure models would place the cluster beyond the Perseus arm, in the inter-arm region. This again favours the distance derived from photometry and the older age.

Xu et al. (2013) assume that the Local arm bends slightly, and branches from the Perseus arm at $\ell \sim 55°$, but we note that a shallower arm curvature would mean a branching point not far from the position of Be 51. There are no known tracers of the Perseus arm between $\ell \approx 50°$ and $\ell \approx 95°$ (Choi et al. 2014), and so Be 51 could represent an important anchoring point for this arm.

4.4 The extent of Be 51

Even if our photometry is deep enough to sample the ZAMS, we are only confidently reaching a spectral type B5 V, corresponding to $M_V \approx -0.8$, and still are unlikely to be complete for the faintest (i.e. more reddened) objects. Even so, we find close to 40 photometric members and a few more possible members down to slightly fainter M_V. If we assume the older age of 60 Ma, these objects are in the range between ~ 4.5 and ~ 6.8 M$_\odot$, i.e. they contribute $\gtrsim 200$ M$_\odot$ to the cluster mass. We cannot attempt to derive an initial mass function (IMF) or a total mass, but by integrating a simple Salpeter law under the assumption that there are 40 stars between 4.5 and 6.8 M$_\odot$, we find a current mass of ~ 1300 M$_\odot$ in stars more massive than the Sun only, simply from this lower limit. This would imply an initial cluster mass $\gtrsim 2000$ M$_\odot$. Integration of a standard (Kroupa 2001) IMF would result in a cluster mass ≈ 4000 M$_\odot$. This is a lower limit that does not take into account the incompleteness of our photometry, the effects of binarity, or dynamical ejections from the cluster. It is clear that Be 51 is at least a moderately massive cluster. As discussed in Section 4.2, comparison to synthetic clusters suggests that a total mass above 5×10^3 M$_\odot$ is needed for the presence of nine evolved stars.

Even though the cluster appears strongly concentrated, there are some very likely members over the whole field covered by our photometry. In addition, even within this small field, there is an indication of increasing reddening towards the north. As mentioned in Section 4.1, the wide-field DSS and 2MASS images strongly confirm this impression. As a further check on the extent of the cluster, we took spectra of some of the luminous red star candidates found outside the cluster core (see Fig. 3 and Table 2). Since we could not observe all objects in the diagram, we selected two stars that lie close ($r < 3$ arcmin) to the cluster but have colours different from those of cluster supergiants, and two stars found at larger distances, with colours similar to cluster members.

The two nearby stars, 501 (2MASS J20114667+3423097) and 502 (2MASS J20114564+3422422), have spectral types M4 Ib and M4 II, respectively. Since they were observed only in the 2007 run, we have no measurement of their radial velocities. The position of star 502 in the CMD clearly rules out an association with the cluster, as it is fainter in K_S than the early-K supergiants. Star 501

also appears too faint, and has a colour excess $E(J - K_S) = 0.67$, lower than cluster members. We thus conclude that these two objects are chance projections.

Star 503 (2MASS J20121264+3420366) lies about 5 arcmin south-east of the cluster. It has exactly the same colours and magnitudes as the clump of early-K supergiants, and its spectral type K2 Ib is typical of this group. Its observed radial velocity, however, $v_{LSR} = -22$ km s^{-1}, is quite different from the cluster average, even though its metallicity is compatible with the cluster average. We note that there are a moderate number of objects with similar colours and magnitudes within 7 arcmin of the cluster that would be worth checking for radial velocities.

Finally, star 901 (2MASS 20115472+3427464) is a very bright infrared source (IRAS 20099+3418) located ~ 3.5 arcmin north of the cluster. It is an M1 Iab supergiant, with a very high colour excess, $E(J - K_S) = 1.37$, very likely due to the dark cloud discussed above. Its *WISE* colours have a very large uncertainty, e.g. $(W1 - W3) = 0.13 \pm 0.26$, but do not suggest a strong intrinsic reddening, associated with heavy mass-loss. Its nature will be discussed in Section 4.7.

4.5 Comparison to previous work

We find a younger age than the few previous works on Be 51. Even though our age estimate is fully supported by the spectral types of the stars observed, it is interesting to consider the reasons why Be 51 had not been identified as a young open cluster before. In the case of Tadross (2008), he obtains an age of 150 Ma, based on 2MASS data. Since the global shape of the isochrones at these ages is similar, the difference is likely due to the distance/age/extinction degeneracy. However, we note that the ages of all young open clusters seem to be overestimated in Tadross (2008). For example, he correctly identifies Berkeley 90 as the youngest cluster in his sample, but he assigns an age of ~ 100 Ma, while it is in fact a very young open cluster containing early-O stars (Marco & Negueruela 2017). This is probably because the only young cluster in his calibration set, Berkeley 55, is given a rather old age of 300 Ma (cf. Negueruela & Marco 2012).

A direct comparison of our photometry with that of Subramaniam et al. (2010) is difficult, as they do not provide coordinates for their objects. However, we can compare ~ 20 bright objects that are easily identifiable in the cluster chart available in the WEBDA data base. There are significant systematic differences between the two photometric data sets. Their V magnitudes are between 0.4 and 0.6 mag brighter than ours, while their $(B - V)$ colours are larger, with their B magnitudes only 0.1 or 0.2 mag brighter than ours. Despite this large difference, inspection of their fig. 22 suggests that the much older age that they give to the cluster is mainly due to an incorrect identification of cluster members, as none of the bright supergiants falls on the isochrone chosen.

4.6 The yellow supergiants

Be 51 is remarkable in containing four F-type supergiants. Only the starburst cluster Westerlund 1 has a larger population (six yellow supergiants), but these are much more massive stars, with ~ 40 M$_\odot$ (Clark et al. 2010). NGC 7790, which is somewhat older than Be 51 (~ 100 Ma; Majaess et al. 2013), hosts three, all of which are Cepheid variables, the two components of the binary CE Cas, and CF Cas. NGC 129, with an age similar to NGC 7790, contains the Cepheid DL Cas and the non-variable F5 Ib supergiant HD 236433. The Cepheid V376 Cas could be a halo member as well (Anderson et al. 2013).

We can use the strength of the O I 7774 Å triplet in the spectra of the F-type supergiants to obtain an independent estimation of the cluster distance, by utilizing the calibration of Arellano Ferro et al. (2003). We measured the strength of the triplet (EW74) on the low-resolution 2007 spectra. The triplet is not resolved, and we estimate an uncertainty of ± 0.1 Å, owing to the definition of the continuum. For star 105, we measure an EW = 1.0 Å, which would correspond to $M_V = -4.9$. For #146, we measure 1.1 Å, i.e. the same value within errors, in good agreement with the fact that the two stars have approximately the same magnitudes and colours in all photometric diagrams. This luminosity is a bit higher than those of α Per or HD 236433, which are quite similar to each other according to Kovtyukh et al. (2012), and have about the same spectral type as the Be 51 objects.

For star 162, however, we measure an EW = 0.6 Å. According to the calibration, this implies an M_V of only -3.0. For #70, we measure a similar EW = 0.7 Å, but this object is likely a binary. Given the position of the two late-F stars in the CMDs, we would expect them to be slightly brighter than the mid-F supergiants, instead of fainter. The most likely explanation resides in the fact that the calibration of Arellano Ferro et al. (2003) does not take into account the dependence of EW74 with effective temperature. According to Kovtyukh et al. (2012), supergiants of later types have weaker EWs at a given luminosity.[10] Moreover, as seen in fig. 3 of Kovtyukh et al. (2012), for temperatures $\sim$6000 K and lower, i.e. as we move into G-types, EW74 seems to show a weaker dependence on luminosity. Star 162 had a spectral type G1 Ib in the spectrum on which EW74 was measured, and therefore falls in this regime. So we have reason to believe that its M_V has been underestimated. We can thus conclude that the values found are consistent, within the uncertainties typical of the calibration (around 0.7 mag), with the isochrones. For the short distance that we have preferred, #105, #146, and #162 have $M_V \approx -4.0$, with #70 somewhat brighter, in agreement with its suspect binary nature. In fact, we would expect that the four yellow supergiants in Be 51, together with those in other clusters containing more than one such object (NGC 129 and NGC 7790 mentioned above), can help improve the calibration, especially once precise *Gaia* distances exist for all of them.

4.7 The nature of IRAS 20100+3415

Star 126 is by far the brightest cluster member in the near-IR. It is also the counterpart of the mid-infrared source IRAS 20100+3415. This object, located in the inner core of the cluster, has a radial velocity fully compatible with other cluster members. However, its late spectral type and position in the CMDs are incompatible with the best-fitting isochrones. As an M2 Iab supergiant, it is expected to be a moderately massive star (typically, of $\sim$15 $M_\odot$). Such objects are extremely rare and a chance coincidence with a young open cluster is very unlikely. Moreover, its luminosity is fully consistent with the expectations for an object of this spectral type at the cluster distance, while the observed $v_{\rm rad}$ makes chance coincidence even more unlikely.

Its *WISE* colours are poorly constrained, probably due to saturation, but with $(W1-W3) = 0.85 \pm 0.29$, there is clear evidence of strong mass-loss. The interpretation of this object is further compounded by the detection of a second luminous supergiant, star 901

---

[10] Note that we have not used the calibration of Kovtyukh et al. (2012) because it has a strong dependence on log g and especially ξ, which we have to fix at assumed values.

discussed above, only $\sim$3.5 arcmin to the north. While K-type supergiants in the Milky Way are generally of luminosity class Ib and can be descended from stars of only 7 or 8 $M_\odot$ (cf. Negueruela & Marco 2012; Alonso-Santiago et al. 2017), M-type supergiants of luminosity class Iab are high-mass stars. Given their short lifetimes, they are rare objects (the known Galactic population runs into the several hundred, with estimates of a total population of a few thousand). Except in regions of intense recent star formation, the chance detection of two such objects within 3.5 arcmin is very unlikely (see Negueruela et al. 2016, for estimates based on actual observations). If we take into account that #126 and #901 have almost identical *dereddened* colours and magnitudes, the possibility that they are not physically related, in spite of a difference in radial velocity of 13 km s^{-1}, seems very unlikely.

If the cluster age lies in the young half of the range considered, the most evolved stars are expected to have, according to isochrones, $\gtrsim 8 M_\odot$. We should then consider the possibility that an object like #126 is a super-asymptotic giant branch (super-AGB) star. The exact mass range at which these objects occur depends on the internal physics (Poelarends et al. 2008) and their expected observational properties are unconstrained. To explore this option, we obtained a high-resolution spectrum of #126 with HERMES, and we scanned its spectrum in search of any indication of AGB nature, such as the presence of the Li I 6708 Å doublet or the Rb I 7800 Å line (e.g. García-Hernández et al. 2007), without finding any of them. We note that the sample of massive AGB stars where these features have been detected have much later spectral types than M2. The spectrum of #126, though, seems indistinguishable from those of other bona fide RSGs of the same spectral type that we had observed at the same resolution. In view of this, we consider that the most likely explanation for the presence of #126 in the cluster is that it is really a more massive star that has formed via mass transfer in an interacting binary. Star 901 would require a more complex explanation, though. Accurate distances to the brightest cluster members in the *Gaia* final release will be able to ascertain this hypothesis.

5 CONCLUSIONS

We have carried out a comprehensive spectroscopic and photometric study of the highly reddened open cluster Be 51. Our analysis conclusively shows that this is a young open cluster with an important population of evolved stars. We identify an MS turn-off at spectral type B3 V and at least two Be stars with earlier spectral types. In addition, we find four yellow and five red supergiants in the central overdensity. Two of the yellow supergiants show spectral variability, displaying spectral types F8 Ib and later, a behaviour typical of Cepheid variables.

A fit to the MS indicates a distance of 5.5 kpc, although we may be missing some of the faintest (most heavily reddened) members. The spectral types of some of the brightest members may favour a higher distance, but both the cluster average radial velocity (when compared to the Galactic rotation curve in this direction) and the strength of the O I triplet in the four yellow supergiants identified support a distance not much higher than 5.5 kpc, which is compatible with a location in the Perseus arm according to most models, even though no other tracers are known in this direction.

Isochrone fits would suggest an age of $\sim$60 Ma for moderate-rotation Geneva models or 65 Ma for PARSEC models. Although the isochrones reproduce well the overall distribution of evolved of stars in the CMDs, the supergiants are not located at positions where the models predict that stars should spend a substantial amount of time. The RSGs (with spectral types G8 or K0) appear all somewhat

warmer than the predictions for the first part of He core burning. Geneva models predict that, after this phase, stars will move to high temperatures and will spend the rest of He core burning as A-type supergiants. The populations observed in a number of clusters with ages ~50 Ma do not seem to agree with this prediction, as they contain preferentially F-type supergiants, either Cepheid variables or objects with stable spectral type close to F5 Ib. The PARSEC isochrones predict shorter blue loops at a given metallicity, which perhaps are in better agreement with observations.

The mid-infrared source IRAS 20100+3415, located near the centre of the cluster, is an M2 Iab supergiant, probably the descendant of a blue straggler formed via binary interaction. Its *WISE* colours suggest heavy mass-loss. Searches for associated maser emission would be of high interest to exploit the availability of Be 51 as a tracer of the Perseus arm in a poorly known region of the Milky Way.

REFERENCES

Aller L. H. et al. eds, 1982, Landolt-Börnstein: Numerical Data and Functional Relationships in Science and Technology – New Series. Springer-Verlag, Berlin

Alonso-Santiago J., Negueruela I., Marco A., Tabernero H. M., González-Fernández C., Castro N., 2017, MNRAS, 469, 1330
Anderson R. I., Eyer L., Mowlavi N., 2013, MNRAS, 434, 2238
Arellano Ferro A., Giridhar S., Rojo Arellano E., 2003, Rev. Mex. Astron. Astrofis., 39, 3
Barklem P. S., Piskunov N., O'Mara B. J., 2000, A&AS, 142, 467
Bressan A., Marigo P., Girardi L., Salasnich B., Dal Cero C., Rubele S., Nanni A., 2012, MNRAS, 427, 127
Carpenter J. M., 2001, AJ, 121, 2851
Cenarro A. J., Cardiel N., Gorgas J., Peletier R. F., Vazdekis A., Prada F., 2001, MNRAS, 326, 959
Chiosi C., Bertelli G., Bressan A., 1992, ARA&A, 30, 235
Choi Y. K., Hachisuka K., Reid M. J., Xu Y., Brunthaler A., Menten K. M., Dame T. M., 2014, ApJ, 790, 99
Clark J. S., Ritchie B. W., Negueruela I., 2010, A&A, 514, A87
Comerón F., Pasquali A., 2005, A&A, 430, 541
Currie M. J., Berry D. S., Jenness T., Gibb A. G., Bell G. S., Draper P. W., 2014, in Manset N., Forshay P., eds, ASP Conf. Ser. Vol. 485, Astronomical Data Analysis Software and Systems XXIII. Astron. Soc. Pac., San Francisco, p. 391
Diaz A. I., Terlevich E., Terlevich R., 1989, MNRAS, 239, 325
Dorda R., González-Fernández C., Negueruela I., 2016, A&A, 595, A105
Draper P. W., Taylor M., Allan A., 2011, Starlink User Note, 139
Dutra-Ferreira L., Pasquini L., Smiljanic R., Porto de Mello G. F., Steffen M., 2016, A&A, 585, A75
Ekström S. et al., 2012, A&A, 537, A146
Ekström S., Georgy C., Meynet G., Groh J., Granada A., 2013, EAS Publ. Ser., 60, 31
Fernie J. D., 1963, AJ, 68, 780
Fitzgerald M. P., 1970, A&A, 4, 234
Foreman-Mackey D., Hogg D. W., Lang D., Goodman J., 2013, PASP, 125, 306
García-Hernández D. A., García-Lario P., Plez B., Manchado A., D'Antona F., Lub J., Habing H., 2007, A&A, 462, 711
Georgy C., Ekström S., 2017, in Charbonnel C., Nota A., eds, Proc. IAU Symp. 316, Formation, Evolution, and Survival of Massive Star Clusters. Cambridge Univ. Press, Cambridge, p. 355
Georgy C., Ekström S., Granada A., Meynet G., Mowlavi N., Eggenberger P., Maeder A., 2013, A&A, 553, A24
González-Fernández C., Negueruela I., 2012, A&A, 539, A100
González-Fernández C., Dorda R., Negueruela I., Marco A., 2015, A&A, 578, A3
Gray R. O., Corbally C. J., 1994, AJ, 107, 742
Gray R. O., Corbally J. C., 2009, Stellar Spectral Classification. Princeton Univ. Press, Princeton, NJ
Gustafsson B., Edvardsson B., Eriksson K., Jørgensen U. G., Nordlund Å., Plez B., 2008, A&A, 486, 951
Harris D. L., III, 1956, ApJ, 123, 371
Howarth I. D., Murray J., Mills D., Berry D. S., 2014, Astrophysics Source Code Library, record ascl:1405.016
Jeffries R. D., 1997, MNRAS, 288, 585
Johnson H. L., 1958, Lowell Obs. Bull., 4, 37
Johnson H. L., Morgan W. W., 1953, ApJ, 117, 313
Kharchenko N. V., Piskunov A. E., Schilbach E., Röser S., Scholz R.-D., 2013, A&A, 558, A53
Koornneef J., 1983, A&A, 128, 84
Koposov S. E. et al., 2011, ApJ, 736, 146
Kovtyukh V. V., Gorlova N. I., Belik S. I., 2012, MNRAS, 423, 3268
Kroupa P., 2001, MNRAS, 322, 231
Kupka F. G., Ryabchikova T. A., Piskunov N. E., Stempels H. C., Weiss W. W., 2000, Balt. Astron., 9, 590
Landolt A. U., 1992, AJ, 104, 340
Maíz Apellániz J. et al., 2015, A&A, 579, A108
Majaess D. et al., 2013, A&A, 560, A22
Mallik S. V., 1997, A&AS, 124, 359
Marco A., Negueruela I., 2017, MNRAS, 465, 784
Marco A., Negueruela I., González-Fernández C., Maíz Apellániz J., Dorda R., Clark J. S., 2014, A&A, 567, A73

Martins F., Plez B., 2006, A&A, 457, 637

Mermilliod J. C., Mayor M., Udry S., 2008, A&A, 485, 303

Meynet G., Maeder A., 2000, A&A, 361, 101

Mowlavi N., Forestini M., 1994, A&A, 282, 843

Negueruela I., 2016, in Benvenuti P., ed., Proc. IAU, Vol. 29B, Astronomy in Focus. Cambridge Univ. Press, p. 461

Negueruela I., Marco A., 2012, AJ, 143, 46

Negueruela I., Schurch M. P. E., 2007, A&A, 461, 631

Negueruela I., Marco A., González-Fernández C., Jiménez-Esteban F., Clark J. S., Garcia M., Solano E., 2012, A&A, 547, A15

Negueruela I., Clark J. S., Dorda R., González-Fernández C., Marco A., Monguió M., 2016, in Skillen I., Barcells M., Trager S., eds, ASP Conf. Ser. Vol. 507, Multi-Object Spectroscopy in the Next Decade: Big Questions, Large Surveys, and Wide Fields. Astron. Soc. Pac., San Francisco, p. 75

Netopil M., Paunzen E., Stütz C., 2012, Astrophysics and Space Science Proceedings, Vol. 29, Star Clusters in the Era of Large Surveys. Springer-Verlag, Berlin, p. 53

Palacios A., Gebran M., Josselin E., Martins F., Plez B., Belmas M., Lèbre A., 2010, A&A, 516, A13

Piskunov N. E., Kupka F., Ryabchikova T. A., Weiss W. W., Jeffery C. S., 1995, A&AS, 112, 525

Poelarends A. J. T., Herwig F., Langer N., Heger A., 2008, ApJ, 675, 614

Raskin G., Van Winckel H., 2014, Astron. Nachr., 335, 32

Reid M. J. et al., 2014, ApJ, 783, 130

Rieke G. H., Lebofsky M. J., 1985, ApJ, 288, 618

Ryabchikova T., Piskunov N., Kurucz R. L., Stempels H. C., Heiter U., Pakhomov Y., Barklem P. S., 2015, Phys. Scr., 90, 054005

Salasnich B., Bressan A., Chiosi C., 1999, A&A, 342, 131

Schaller G., Schaerer D., Meynet G., Maeder A., 1992, A&AS, 96, 269

Shortridge K., Meyerdierks H., Currie M. J., Davenhall C., Jenness T., Clayton M., 2014, Astrophysics Source Code Library, record ascl:1411.022

Skrutskie M. F. et al., 2006, AJ, 131, 1163

Stetson P. B., 1987, PASP, 99, 191

Subramaniam A., Carraro G., Janes K. A., 2010, MNRAS, 404, 1385

Tabernero H. M., Dorda R., Negueruela I., González-Fernández C., 2018, MNRAS, 476, 3106

Tadross A. L., 2008, MNRAS, 389, 285

Turner D. G., 1980, ApJ, 240, 137

Weidemann V., 2000, A&A, 363, 647

Winkler H., 1997, MNRAS, 287, 481

Xu Y. et al., 2013, ApJ, 769, 15

van Leeuwen F., 2009, A&A, 497, 209

SUPPORTING INFORMATION

Supplementary data are available at *MNRAS* online.

APPENDIX A: SYNTHETIC CLUSTERS
APPENDIX B: PHOTOMETRIC DATA

Please note: Oxford University Press is not responsible for the content or functionality of any supporting materials supplied by the authors. Any queries (other than missing material) should be directed to the corresponding author for the article.

This paper has been typeset from a TEX/LATEX file prepared by the author.